

Memory-based optical polarization conversion in a double- Λ atomic system with degenerate Zeeman states

Yan-Cheng Wei^{1,2}, Sheng-Xiang Lin^{1,2}, Pin-Ju Tsai^{1,2}, and Ying-Cheng Chen^{1,3*}

¹Institute of Atomic and Molecular Sciences, Academia Sinica, Taipei 10617, Taiwan

²Department of Physics, National Taiwan University, Taipei 10617, Taiwan

³Center for Quantum Technology, Hsinchu 30013, Taiwan

*chenyc@pub.iams.sinica.edu.tw

ABSTRACT

Optical memory based on electromagnetically induced transparency (EIT) in a double- Λ atomic system provides a convenient way to convert the frequency, bandwidth or polarization of optical pulses by storing in one Λ channel and retrieving in another. This memory-based optical converter can be used to bridge quantum nodes of different physical properties in a quantum network. However, in real atoms, each energy level usually contains degenerate Zeeman states and this may lead to additional energy loss, as have been discussed in our recent theoretical paper (Phys. Rev. A 100, 063843). Here, we present an experimental study on the efficiency variation in the EIT-memory-based optical polarization conversion in cold cesium atoms under the Zeeman-state optical pumping. The experimental results support the theoretical predictions. Our works provide quantitative knowledge and physical insight useful to the practical implementation of EIT-memory-based optical converter.

Introduction

Storage and retrieval of light pulses in atomic ensembles using the effect of electromagnetically induced transparency (EIT) in a three-level system have been intensively studied due to its important application as quantum memory for quantum information processing^{1,2}. By controlling the intensity, frequency or direction of the control field during the retrieval process, the temporal width, frequency or propagating direction of the retrieved probe pulses can be manipulated³⁻⁶. With a four-level double- Λ system, the wavelength of the retrieved probe pulses can be widely manipulated by turning on the control field of the second Λ system during retrieval process⁶⁻⁹. This can be served as a quantum frequency converter to interface different quantum systems in a quantum network. Furthermore, by turning on both control fields during retrieval, the stored atomic coherence can be simultaneously released into two separate photonic channels with the amplitude ratio controlled by the intensity ratio of the two control fields^{5,7,8,10}. This can be served as a frequency-domain tunable beam splitter¹¹ or two-color quantum memory¹².

However, each energy level usually contains degenerate Zeeman states in real atoms and this may induce some complications in the memory-based optical conversion with a double- Λ system. In a recent theoretical work¹³, we have performed such a study and identified the two factors affecting the efficiency of the converted pulses. The first factor is the finite bandwidth effect of the optical pulses and the difference in the optical depth of the storage and retrieval channels. The second factor is the incompatibility between the stored ground-state coherence and the ratio of the probe and control Clebsch-Gordan coefficients, which lead to a nonadiabatic energy loss in the retrieved pulses^{6,7,14}. We obtained an approximate relation for the conversion efficiency. Besides, we also numerically study the dependence of those two factors on the Zeeman population distribution, prepared by optical pumping¹³.

In this paper, we conduct an experimental study on the EIT-memory-based optical polarization conversion in a double- Λ system with degenerate Zeeman states using cold cesium atoms. Specifically, we study the dependence of the conversion efficiency on various configurations, including the Zeeman population distribution prepared by optical pumping, the pulsed or continuous-wave probe, and the difference in optical depth for the storage and retrieval channel. The experimental observations support the experimental predictions. Our work provides useful quantitative knowledge and insight in the optical conversion based on EIT-memory.

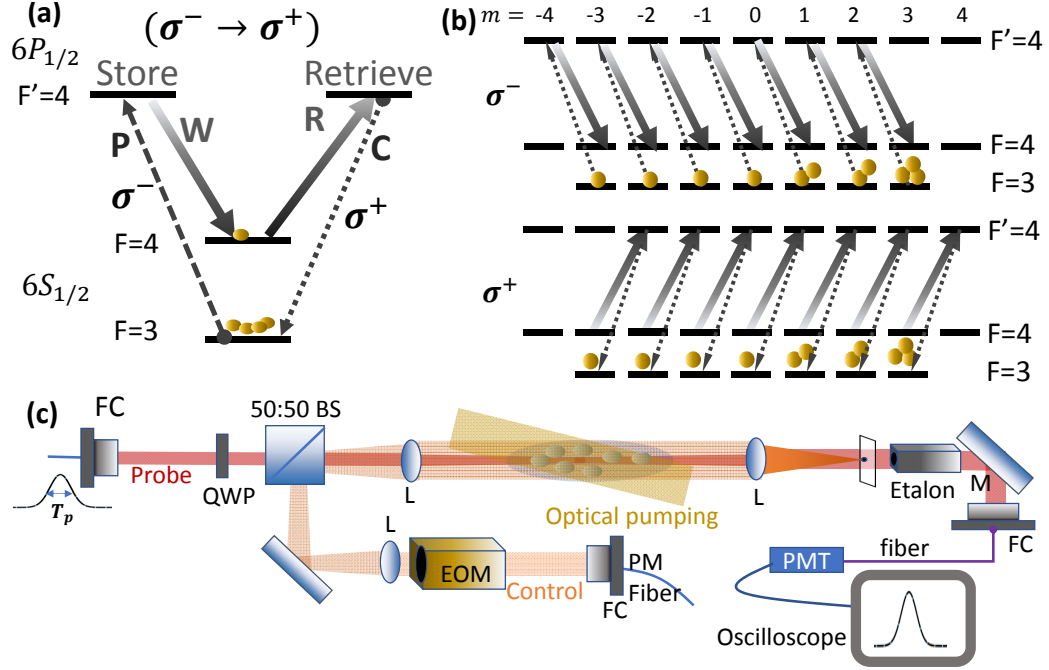


Figure 1. (a) Relevant energy levels for ^{133}Cs atoms and laser excitations. In this figure, we plot the case to store light into the spin-wave with a left-hand circularly polarized beam (σ^- transition) and to retrieve with a right-hand circularly polarized beam (σ^+ transition). W,R,P,C denote writing control, reading control, probe, conversion fields, respectively. This case and the opposite case, i.e. storing by the σ^+ transitions and retrieving by the σ^- transitions, are both implemented in the experiment. (b) The complete energy levels and laser excitations considering the degenerate Zeeman states. (c) Schematic experimental setup. BS: beam splitter; M: mirror; L: lens; FC: fiber coupler; QWP: quarter waveplate; PMT: photo-multiplier tube; EOM: electro-optic modulator; PM fiber: polarization-maintaining fiber;

Results

Theoretical Model

Before mentioning the experiment, we briefly give a summary on the theoretical background¹³. We consider the EIT-memory-based optical polarization conversion in a double- Λ system with degenerate Zeeman states as shown in Fig.1a and b for cesium D_1 line. In the $\sigma^- \rightarrow \sigma^+$ ($\sigma^+ \rightarrow \sigma^-$) conversion system, both the probe and writing control beams drive the σ^- (σ^+) transitions in the storage channel and the conversion and reading control fields drive the σ^+ (σ^-) transitions in the retrieval channel. We focus our discussion on the relative conversion efficiency, ξ_c^R , which is defined as the energy ratio of the conversion pulse to that retrieved in the original storage channel. With this definition of ξ_c^R , the efficiency during the storage process has been normalized away. Based on Maxwell-Bloch equations and under certain approximations, we obtain¹³

$$\xi_c^R = \xi_1(\eta) \xi_2, \quad \xi_1(\eta) = \frac{\zeta_p(\eta)}{\zeta_c(\eta)}, \quad \xi_2 = \frac{|\sum_j p_j R_j^p R_j^c|^2}{\sum_j p_j R_j^{p2} \sum_j p_j R_j^{c2}}, \quad (1)$$

where ζ_p, ζ_c are given by

$$\zeta_p(\eta) = \left[1 + \frac{16 \ln 2 (\eta - \kappa) \eta \sum_j p_j R_j^{p4} / (a_{p,j}^2 \alpha_p)}{\beta_w^2(L_w) (\sum_j p_j R_j^{p2})^2} \right]^{\frac{1}{2}}, \quad \zeta_c(\eta) = \left[1 + \frac{16 \ln 2 (\eta - \kappa) \eta \sum_j p_j R_j^{c4} / (a_{c,j}^2 \alpha_c)}{\beta_w^2(L_w) (\sum_j p_j R_j^{c2})^2} \right]^{\frac{1}{2}}, \quad (2)$$

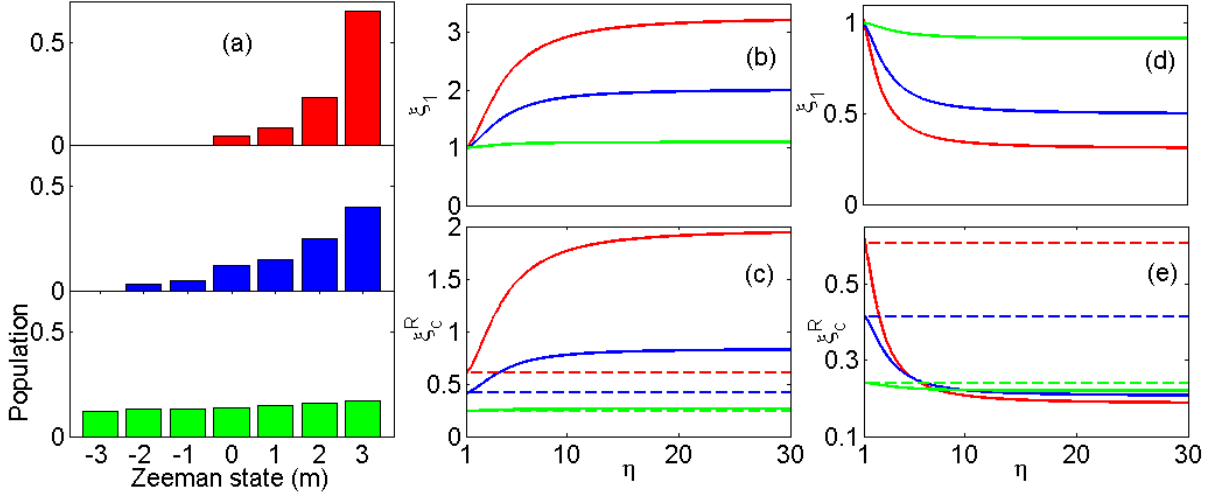


Figure 2. Theoretical calculations based on Eq. 1. (a) Three assumed Zeeman population distributions. The Zeeman population changes from near isotropic distribution towards mostly concentrated in the rightmost Zeeman state from bottom to top. The optical depth for the probe driving the σ^+ (σ^-) transition increases (decreases) from the bottom population to the top one. The solid curves in (b, c) ((d, e)) are ξ_1 and ξ_c^R versus η for the $\sigma^- \rightarrow \sigma^+$ ($\sigma^+ \rightarrow \sigma^-$) conversion system. The color of the curves indicates the corresponding Zeeman population of (a) used in the calculation. The dash lines in (c) and (e) of the same color are the corresponding ξ_2 . The parameters $\alpha_p = \alpha_c = 500$ and $\kappa = 1.1$.

and

$$\beta_w(L_w) = [1 + 16 \ln 2 \frac{\eta \kappa}{D_p}]^{\frac{1}{2}}, \quad (3)$$

where $R_j^p = \frac{a_{p,j}}{a_{w,j}}$, $R_j^c = \frac{a_{c,j}}{a_{r,j}}$, $\eta \equiv \frac{T_d}{T_p}$, $\kappa \equiv \frac{T_w}{T_d}$, and $L_w = v_w T_w \simeq T_w L / T_d = L \kappa / \eta$. v_w is the group velocity of the probe pulse in the storage channel. All subscripts j denote the j^{th} Zeeman sub-level, and p_j denotes population in the j^{th} ground state of the probe transition; $a_{(p,c,r,w)}$ denote Clebsch-Gordan coefficients for the probe, conversion, reading control, and writing control fields, respectively. α_p and α_c are the normalized optical depth of the probe and conversion transition without multiplied by the Clebsch-Gordan coefficients. The actual optical depths are $D_{(p;c)} = \sum_j \alpha_{(p;c)} a_{(p;j;c,j)}^2$. T_d denotes group delay time of the slow light and can be expressed as $D_p \Gamma / \Omega_w^2$, where Ω_w is the Rabi frequency of the writing control field, and Γ denotes the spontaneous decay rate; T_w denotes the time when the writing control beam is switched off; T_p denotes intensity full width at half maximum (FWHM) of the input probe pulse with a Gaussian waveform.

In Eq. 1, the relative conversion efficiency is determined by the product of two factors, which we term as the finite bandwidth factor (ξ_1) and the ground-state coherence mismatch factor (ξ_2)¹³. ξ_2 , ranging from zero to unity, stands for a nonadiabatic energy loss during the retrieval process when the population is distributed among several Zeeman states and a mismatch exists on the ratio R_j^p / R_j^c for any of the j^{th} sub-system^{13,14}. The other factor ξ_1 is due to the finite bandwidth effect of the optical pulse and the difference in optical depth between the storage and retrieval channels¹³. In the pulsed probe case, ξ_1 depends on the parameter $\eta = T_d / T_p = D_p \Gamma / (\Omega_w^2 T_p)$. Because the EIT bandwidth of the storage channel $\Delta \omega_{EIT} \propto \Omega_w^2 / (\sqrt{D_p} \Gamma)$ and the spectral bandwidth of the probe pulse $\Delta \omega_p \propto 1 / T_p$, $\eta \propto \sqrt{D_p} \Delta \omega_p / \Delta \omega_{EIT}$, which is related to the ratio of the pulse bandwidth to EIT bandwidth¹⁵. This is why we call ξ_1 the finite-bandwidth factor. To have a clear picture of the trend based on Eq. 1, Fig. 2 (b,c) and (d,e) depict a theoretical plot for ξ_1 and ξ_c^R versus η for the $\sigma^- \rightarrow \sigma^+$ and $\sigma^+ \rightarrow \sigma^-$ conversion system, respectively. The three solid curves (red, blue and green) in Fig. 2(b,c) and (d,e) correspond to the three Zeeman population distributions shown in Fig. 2 a of the same color. The three dash lines in (c,e) are the corresponding ξ_2 , which are independent of η . Some trends are noted. First, ξ_1 is larger (smaller) than unity for the $\sigma^- \rightarrow \sigma^+$ ($\sigma^+ \rightarrow \sigma^-$) conversion system. As discussed in Ref.¹³, the retrieval efficiency is related to the delay-bandwidth product of the retrieved transition, which is dependent on the optical depth only. The retrieval channel with a larger optical depth has a higher retrieval efficiency. Considering the Clebsch-Gordan coefficients for cesium D_1 transition and the assumed Zeeman population, the $\sigma^- \rightarrow \sigma^+$ ($\sigma^+ \rightarrow \sigma^-$) conversion system corresponds to the conversion from a channel with a smaller (larger) optical depth to that with a larger (smaller) one. Second, the deviation of ξ_1 from unity is larger for the Zeeman population with a more concentrated distribution towards the $|m = 3\rangle$ state. This is due to a larger contrast in the Clebsch-Gordan coefficient for the σ^- and σ^+ probe transitions for the Zeeman

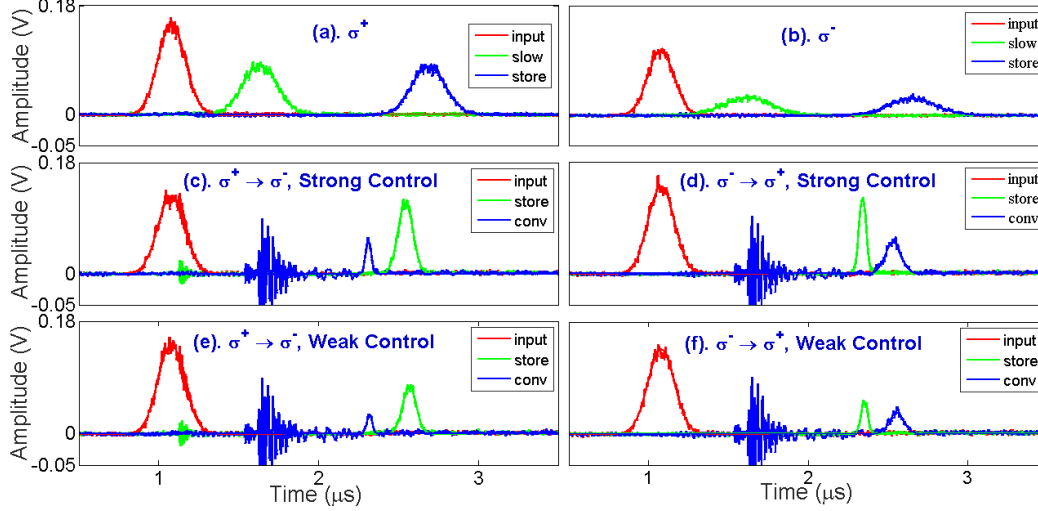


Figure 3. Representative raw data. (a) and (b) depict the input (red), slowed (green), and stored and retrieved (blue) probe pulses in the same EIT channel: σ^+ and σ^- channel, respectively. (c,e) and (d,f) depict the input (red), stored and retrieved in the original channel (green), and the converted (blue) pulses in the $\sigma^+ \rightarrow \sigma^-$ and $\sigma^- \rightarrow \sigma^+$ conversion system, respectively. The intensities of the writing control beams for (c) and (d) are stronger than those of (e) and (f), respectively. The Rabi frequencies for the writing control beam (Ω_w) are (a) 4.03Γ , (b) 1.97Γ , (c) 3.11Γ , (d) 1.51Γ , (e) 2.11Γ , and (f) 0.93Γ , respectively. The relative conversion efficiency (ξ_c^R) are (c) 17.4%, (d) 93.8%, (e) 15.4%, and (f) 150.5%, respectively. The high frequency noises appearing in (c,d,e,f) at roughly $1.7\ \mu\text{s}$ come from the electronic noises due to the switching-on of the high voltage power supply for electro-optic modulator. The optical depths for the σ^+ and σ^- EIT system are 389(41) and 52(3), respectively, where the quantity in the bracket is the 2σ standard deviation.

state with a larger m quantum number. In the case with isotropic Zeeman population, the overall transition dipole moment for the σ^- and σ^+ probe transition are equal and thus ξ_1 is equal to unity. Third, ξ_2 increases with a more concentrated Zeeman distribution and is actually equal to unity when all population are in a single Zeeman state¹³. Fourth, although $\xi_1 > 1$ for the $\sigma^- \rightarrow \sigma^+$ system but $\xi_c^R (= \xi_1 \xi_2)$ is larger than unity only if the Zeeman population is concentrated enough and if η is larger than a certain value, as shown in Fig.2c. Even though the relative conversion efficiency is larger than unity, this situation occurs at a relatively large η such that the absolutely conversion efficiency is significantly less than unity. Fifth, ξ_1 approaches unity when η decreases for both $\sigma^- \rightarrow \sigma^+$ and $\sigma^+ \rightarrow \sigma^-$ conversion system. A smaller η corresponds to a stronger writing control field and thus a wider EIT transparent bandwidth, compared to the spectral bandwidth of the probe pulse. The finite-bandwidth effect is thus less significant.

Experimental Details

Our experiment is based on a cesium magneto-optical trap (MOT) with optically dense cold atomic media. Details of the MOT and experimental setup can be referred to Refs.^{15,16}. The relevant energy levels and laser excitations are shown in Fig.1a. For the storage channel, the writing control field and the probe field drive the $|F=4\rangle \rightarrow |F'=4\rangle$ and $|F=3\rangle \rightarrow |F'=4\rangle$ σ^- transition of cesium D_1 line, respectively. For the retrieval channel, the reading control field and the conversion field drive the same transitions but with σ^+ polarizations, as shown in Fig.1a. We compare this conversion system with that of the opposite driving case, i.e., storing with σ^+ transitions and retrieving with σ^- transitions. Each hyperfine level in Fig.1a contains multiple degenerate Zeeman states. The complete laser excitations are shown in Fig.1b. In this experiment, we manipulate the polarization of the retrieved light but not its frequency. Although it is also possible to manipulate the frequency of the retrieved pulses by choosing another control transition during the retrieval process, our scheme allows us to concentrate our study on the relative efficiency change of the retrieved pulses without bothering by the systematic effects due to the detection of retrieved pulses of different wavelength.

The schematic setup of the experiment is shown in Fig.1c. The probe beam doubly passes through one acoustic-optic modulator (AOM) for tuning its frequency and then passes through another AOM for shaping its temporal waveform into a Gaussian pulse. In the pulsed probe experiment, the full width at half maximum (FWHM) of the Gaussian probe pulse (denoted as T_p) is set to 200 ns. We also conduct the storage and retrieval experiment with a continuous-wave (CW) probe for a comparison with the pulsed probe case. More details of the CW probe experiment are described in Methods section. The probe beam is sent into the MOT cell via a polarization-maintaining fiber. The control beam passes through an electro-optic modulator

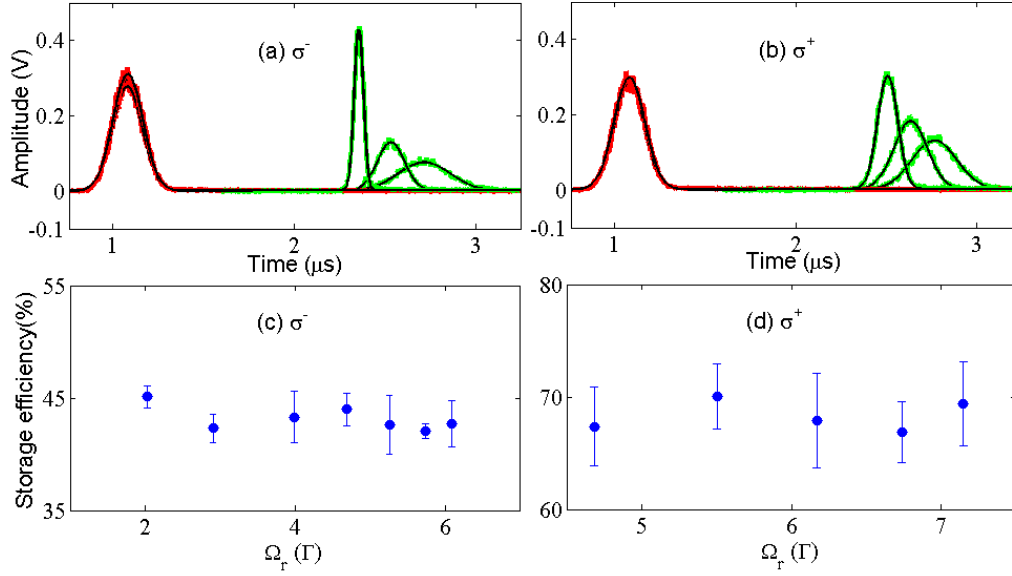


Figure 4. (a) and (b) depict representative data of the stored and retrieved pulses (green) for some intensities of the reading control beam in the σ^+ and σ^- channel, respectively. The red trace is the input pulse. All black solid lines are the Gaussian fits to the data. In (a), the Rabi frequency of the writing control beam Ω_r are 2.02, 2.90 and 6.09 Γ . In (b), the Ω_r are 4.68, 5.50, and 6.74 Γ . (c) and (d) depict the storage efficiency versus Ω_r for the σ^- and σ^+ channel, respectively. The optical depth of the σ^+ and σ^- EIT system are 349(32) and 47(3), respectively.

(EOM) to quickly change its polarization within ~ 10 ns after the storage and before the retrieval process. It then couples with the probe beam together through a beam splitter before entering the atomic clouds. The probe beam is focused to an intensity e^{-2} diameter of $\sim 100\mu\text{m}$ around the atomic clouds while the control beam is collimated with a diameter of ~ 1 mm. After coming out of the MOT cell, both beams pass through another lens and the control beam is focused while the probe beam is collimated. The control beam is blocked by a window with a black dot in the focal plane. The probe beam passes through three irises and an etalon filter, before coupled into a fiber and detected by a photomultiplier tube (Hamamatsu R636-10).

To control the ground-state coherence mismatch factor (ξ_2), which is sensitive to the Zeeman population distribution, we apply an optical pumping beam which drives the D_2 line $|F = 3\rangle \rightarrow |F' = 2\rangle$ σ^+ transitions¹⁵. It pumps atomic population toward the Zeeman states with larger magnetic quantum number m . We can control the Zeeman population distribution by the duration and/or intensity of the optical pumping beam. The Zeeman population can be determined by the microwave spectroscopy, described in the Methods section.

Experimental Observations

We demonstrate the representative raw data in Fig.3. In all these measurements, the optical pumping beam is applied for $20\mu\text{s}$ to pump atoms towards the $|F = 3, m = 3\rangle$ state. Fig.3a and Fig.3b depict the input, slowed, and stored and retrieved optical pulses in the same Λ system (σ^+ and σ^- , respectively). In order to achieve an optimized retrieval efficiency, we adjust the power of the control beam such that $\eta = T_d/T_p \approx 2.7$ ¹⁵. Since the optical depth of the atomic clouds corresponding to the σ^+ channel is larger than that of the σ^- channel under the optical pumping condition, the measured efficiencies of the slow light (67 %) and stored light (66 %) in the σ^+ EIT channel are larger than those (49 %, 45 %) of the σ^- EIT channel¹⁵.

In the following, we present the data with polarization conversion. Fig.3c and Fig.3e (Fig.3d and Fig.3f) correspond to the case of storing via σ^+ channel (σ^- channel) and retrieving via σ^- channel (σ^+ channel). Both Fig.3c and Fig.3d store via stronger writing control field, compared to those of Fig.3e and f which use weaker writing control field. The finite bandwidth factor ξ_1 should be less than unity in the $\sigma^+ \rightarrow \sigma^-$ conversion case, since it converts from the channel with a larger optical depth into that with a smaller one. Also, the coherence mismatch factor ξ_2 for this conversion case is smaller than unity because the Zeeman population is not completely in a single Zeeman state and the Clebsch-Gordan coefficients mismatch exist between the two Λ systems. Thus, the relative conversion efficiency ξ_c^R is smaller than unity based on Eq.1, which agrees with both Fig.3c and Fig.3e. In the case of Fig.3e with a weaker writing control field and thus a larger η , ξ_1 decreases further because of a stronger finite bandwidth effect and this leads to an even smaller ξ_c^R . In the opposite case of $\sigma^- \rightarrow \sigma^+$ conversion, the ξ_1 factor is larger than unity since it converts from the system of a smaller optical depth into that of a larger one. However, the ξ_2 factor is still smaller than unity and these two factors compete against each other. In the case with a stronger writing

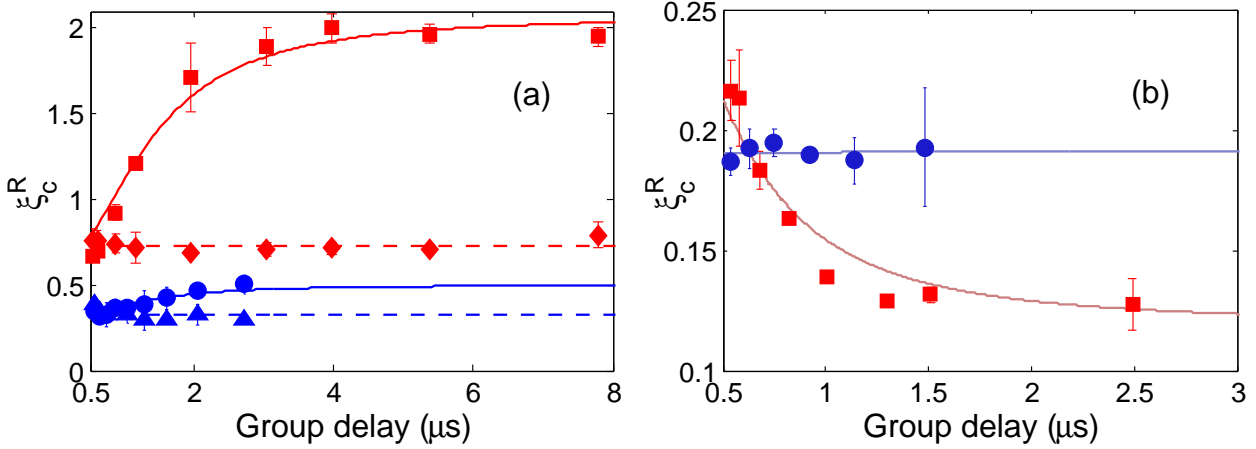


Figure 5. Relative conversion efficiency ξ_c^R versus group delay time of the storage process for (a) $\sigma^- \rightarrow \sigma^+$ and (b) $\sigma^+ \rightarrow \sigma^-$ conversion system. In (a), the red square (diamond) data corresponds to the pulsed (continuous) probe case with Zeeman optical pumping which pumps population towards the $m=3$ state. The blue circle (triangle) data corresponds to the pulsed (continuous) probe case without Zeeman optical pumping. The two dash lines correspond to the average values of ξ_c^R for the continuous case. The two solid curves are the calculation by Eq.1 with $\alpha_p=\alpha_c=1600$, $\kappa=1.5$, and the population from $|F=3, m=3\rangle$ to $|F=3, m=-3\rangle$ states to be (0.56, 0.27, 0.13, 0.04, 0, 0, 0) and (0.25, 0.25, 0.15, 0.15, 0.10, 0.05, 0.05) for the case with and without Zeeman optical pumping, respectively. In (b), the red square (blue circle) data correspond to the pulsed probe case with and without optical pumping. The population from $m=3$ to -3 states are (0.52, 0.24, 0.08, 0.04, 0.03, 0.02, 0.07) and (0.19, 0.17, 0.11, 0.10, 0.07, 0.17, 0.20), respectively. The two solid lines are the calculation by Eq.1 with $\kappa=1.1$ and $\alpha_p=\alpha_c=400$.

control regime (and thus a smaller η), the finite bandwidth effect is relatively less significant and ξ_c^R is mainly affected by the coherence mismatch factor ξ_2 . Thus, the overall ξ_c^R is still smaller than unity, corresponding to the case of Fig.3d. In the case with a weaker writing control beam (and thus a larger η), the finite bandwidth effect dominates and ξ_1 could be larger than unity. Therefore, the overall ξ_c^R could be larger than unity for a large enough η , such as that of Fig.3f. In this case, the efficiency of the converted light is even larger than that retrieved in the original channel. Although the relative conversion efficiency ξ_c^R could be larger than unity, the absolute conversion efficiency is significantly lower than unity since $\xi_c^R > 1$ occurs at a relatively large η and in that case the efficiency of the storage process is relatively low.

It should be noted that the pulse height and temporal width of the retrieval signal can be manipulated by the intensity of the reading control beam (with its Rabi frequency denoted as Ω_r)^{4,5}. In an ideal three-level Λ -type EIT system, the retrieval efficiency should be independent of Ω_r ¹⁷. However, in real atom, there may exist nearby transitions such that the off-resonant excitation of the control beam may induce a Ω_r -dependent multi-photon decay of the spin-wave^{15,18}. Fortunately, the nearest off-resonant excitation of the control field for cesium D_1 line is quite far-detuned (~ 1.167 GHz for the $|6S_{1/2}, F=4\rangle \rightarrow |6P_{1/2}, F=3\rangle$ transition) such that the decay of the spin-wave due to the above-mentioned mechanism is negligible, at least for low Ω_r ¹⁵. To check if this is true, we measure the retrieval efficiency with different Ω_r for both the σ^- and σ^+ EIT systems, as shown in Fig.4. Within the experimental uncertainty, the retrieval efficiencies are roughly a constant for the range of used Ω_r . This trend may not be valid if one implement the EIT-memory-based using the D_2 transition¹⁵. Because of this fact and in order to make the retrieval signal more clear, we choose a relatively strong reading control field to retrieve the signal, such as those shown in Fig.3.

To gain a more comprehensive picture, we conduct systematic measurements of ξ_c^R versus η by varying the Ω_w for various configurations. In the measurements, we all keep $T_p=200$ ns. We consider both the $\sigma^- \rightarrow \sigma^+$ and $\sigma^+ \rightarrow \sigma^-$ conversion system, which corresponding to storing in a system with smaller optical depths and retrieving in another system with larger optical depths and the opposite. In each system, we also consider to vary the Zeeman population distribution by applying optical pumping beam or not. To explore the finite bandwidth effect, we also consider the storage and retrieval with a continuous-wave (CW) probe to serve as a reference for the pulsed probe case.

Fig.5a depicts the results for the $\sigma^- \rightarrow \sigma^+$ conversion system. The red square and blue circle are the data of the pulsed probe case with Zeeman optical pumping on and off, respectively. The red diamond and blue triangle are the data corresponding to the case of CW probe. It is evident that ξ_c^R for the CW case almost show no dependence on the group delay time T_d . This is not surprising since the finite-bandwidth effect in the CW case is negligible and ξ_c^R is only determined by ξ_2 . Without optical

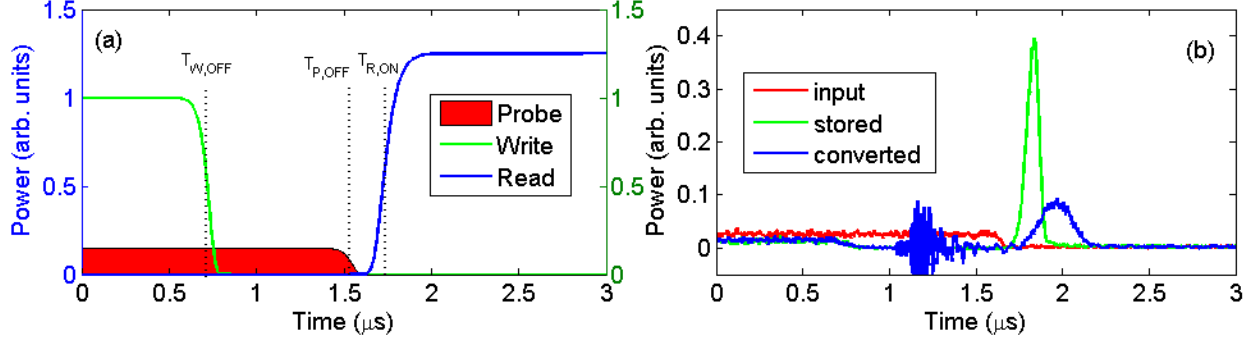


Figure 6. (a) The schematic timing diagram for the probe (red), writing control (green) and reading control (blue) fields to implement the continuous probe storage and conversion measurement. The reading control beam could be that of the original Λ channel or the converted Λ channel. (b) One representative data for the input continuous probe (red), the retrieved probe fields in the original (green) and in the converted (blue) Λ channel. The noises around $1.2 \mu\text{s}$ are due to the switching on of the high-voltage driver for EOM.

pumping, Zeeman population is nearly isotropic and the ξ_c^R shows a very weak dependence on η . With optical pumping, the Zeeman population concentrated towards Zeeman states with a larger m and ξ_c^R increases with η . At a large enough T_d , ξ_c^R is larger than unity and approaches to a maximum value of ~ 2 at large T_d . For the CW probe case, ξ_c^R is larger for the case with optical pumping because the Zeeman population is more concentrated which favors a larger ξ_2 . All these behaviors are similar to the theoretical predictions of Fig.2 and have been explained in the theory section.

We next conduct the corresponding experiments of the $\sigma^+ \rightarrow \sigma^-$ conversion system, with the results shown in Fig.5b. Here, opposite to the previous case, the light is converted from the system with a large optical depth to that with a small one. The finite bandwidth factor ξ_1 is thus less than unity, which results in the decrease of ξ_c^R when T_d increases. This behavior is more significant when the optical pumping is on and the Zeeman population concentrated towards the Zeeman states with a larger m . ξ_c^R becomes insensitive to T_d when the optical pumping is off and the Zeeman population is more close to an isotropic distribution. The behaviors are similar to the theoretical predictions.

Conclusion

We conduct an experiment on EIT-memory-based optical polarization conversion in a double- Λ system with cold cesium atoms. The dependence of the conversion efficiency on the degenerate Zeeman states and finite bandwidth effect have been studied. The experimental observations support the theoretical predictions. Our studies provide essential knowledge for the practical implementation of EIT-memory-based optical converter.

Methods

Measurement of the continuous-wave (CW) conversion efficiency

To implement the storage and conversion of the continuous-wave (CW) probe field, we firstly turn on both the writing control beam and the probe beam. The probe power is kept at a constant value. The writing control beam is switched off at a given time (denoted as $T_{W,OFF}$). After a certain time, the probe beam is also turned off (denoted as $T_{P,OFF}$). This ensure that the atomic ensemble is filled by a certain portion of the probe beam of constant intensity such that its behavior is more like the CW case. At time $T_{W,OFF}$, the portion of probe beam that enters the atomic medium will be converted to and stored as the spin-wave. Other parts of the probe beam that enter the medium later than $T_{W,OFF}$ will be absorbed. At a time (denoted as $T_{R,ON}$) later than $T_{P,OFF}$, the writing control beam, either of the original Λ system or the converted one, is turned on to retrieve the probe pulse in the original Λ system or in the converted Λ system, respectively. The schematic timing diagram is shown in Fig.6a. One representative data of such measurement is shown in Fig.6b. The ratio of the retrieved probe energy in the converted Λ system (blue) to that in the original Λ system (green) is the relative conversion efficiency of the CW case.

Determination of the Zeeman population by microwave spectroscopy

To determine the Zeeman population distribution, we conduct the microwave spectroscopy. In the measurement, we apply a magnetic field of $\approx 248\text{mG}$ and turn on a microwave pulse of $50 \mu\text{s}$ duration through a horn antenna to drive atoms from the $|6S_{1/2}, F=3\rangle$ Zeeman states into the $|6S_{1/2}, F=4\rangle$ Zeeman states. The trapping beams are then turned on with its frequency

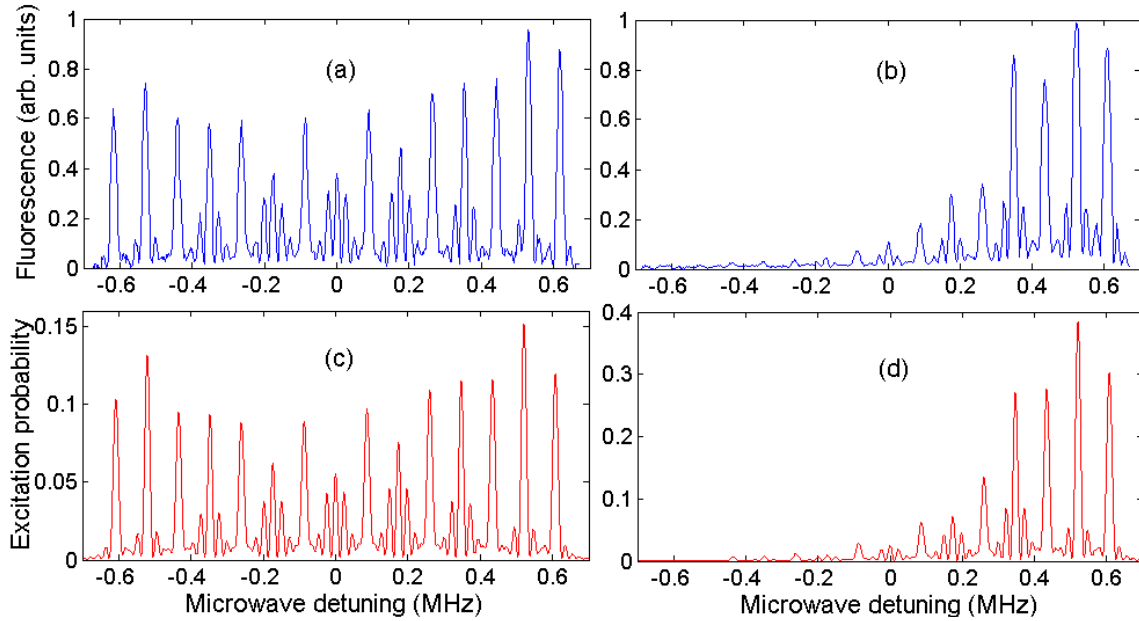


Figure 7. (a) and (b) are the representative microwave spectrum with Zeeman optical pumping off and on, respectively. The x-axis is the microwave frequency minus 9192.63177 MHz, the hyperfine splitting between the $|F = 3\rangle$ and $|F = 4\rangle$ ground state. (c) and (d) are the calculated microwave spectrum corresponding to (a) and (b) with population from $|m = 3\rangle$ to $|m = -3\rangle$ to be (0.15, 0.16, 0.16, 0.14, 0.13, 0.13, 0.13) and (0.38, 0.38, 0.15, 0.06, 0.02, 0.01, 0), respectively. In the calculation, the magnetic field is 248 mG. The microwave Rabi frequencies for the π transitions are 3.936×10^5 Hz, multiplied by the Clebsch-Gordan coefficients. The Rabi frequency ratio for the microwave σ to π transition is 0.36, which is related to the angle between the microwave magnetic field to the applied DC magnetic field.

jumped to resonance of the $|6S_{1/2}, F = 4\rangle \rightarrow |6P_{3/2}, F' = 5\rangle$ cycling transition. One CCD camera is then used to collect the atomic fluorescence for $70 \mu\text{s}$. The microwave frequency is scanned through 9.192 GHz and the timing sequence repeat to get the spectrum. There are 15 major lines appear in the spectrum due to the Zeeman shifts with an example shown in Fig. 7a and b with the Zeeman optical pumping off and on, respectively. Some lines are split into several sub-lines due to the relatively strong microwave field used for the experiment. Because the total trapping laser intensity is very strong ($\sim 100 \text{ mW/cm}^2$ corresponding to an on-resonance saturation parameter of ~ 37 with respect to the isotropic saturation intensity of 2.706 mW/cm^2)¹⁹, the fluorescence rate for each Zeeman sublevel is almost saturated to $\Gamma/2$ and the relative intensities of the spectral peaks are determined by the Zeeman population and the relative strength of the microwave transition only. By varying the microwave Rabi frequency, the Rabi frequency ratio between the microwave π to σ transition and the Zeeman population, the calculated microwave spectrum resembles the experimental spectrum very well, as shown in Fig. 7c and d. As shown in Fig. 7d, the σ^+ optical pumping beam do pump the Zeeman population towards the Zeeman states with larger magnetic quantum number m .

References

1. Fleischhauer, M. & Lukin, M. D. Dark-state polaritons in electromagnetically induced transparency. *Phys. Rev. Lett.* **84**, 5094–5097, DOI: [10.1103/PhysRevLett.84.5094](https://doi.org/10.1103/PhysRevLett.84.5094) (2000).
2. Fleischhauer, M. & Lukin, M. D. Quantum memory for photons: Dark-state polaritons. *Phys. Rev. A* **65**, 022314, DOI: [10.1103/PhysRevA.65.022314](https://doi.org/10.1103/PhysRevA.65.022314) (2002).
3. Zibrov, A. S. *et al.* Transporting and time reversing light via atomic coherence. *Phys. Rev. Lett.* **88**, 103601, DOI: [10.1103/PhysRevLett.88.103601](https://doi.org/10.1103/PhysRevLett.88.103601) (2002).
4. Patnaik, A. K., Kien, F. L. & Hakuta, K. Manipulating the retrieval of stored light pulses. *Phys. Rev. A* **69**, 035803, DOI: [10.1103/PhysRevA.69.035803](https://doi.org/10.1103/PhysRevA.69.035803) (2004).
5. Chen, Y.-F., Wang, S.-H., Wang, C.-Y. & Yu, I. A. Manipulating the retrieved width of stored light pulses. *Phys. Rev. A* **72**, 053803, DOI: [10.1103/PhysRevA.72.053803](https://doi.org/10.1103/PhysRevA.72.053803) (2005).

6. Chen, Y.-F., Kuan, P.-C., Wang, S.-H., Wang, C.-Y. & Yu, I. A. Manipulating the retrieved frequency and polarization of stored light pulses. *Opt. Lett.* **31**, 3511–3513, DOI: [10.1364/OL.31.003511](https://doi.org/10.1364/OL.31.003511) (2006).
7. Raczynski, A. & Zaremba, J. Controlled light storage in a double- Λ system. *Opt. Commun.* **209**, 149 – 154, DOI: [https://doi.org/10.1016/S0030-4018\(02\)01642-5](https://doi.org/10.1016/S0030-4018(02)01642-5) (2002).
8. Raczynski, A., Zaremba, J. & Zielińska Kaniasty, S. Electromagnetically induced transparency and storing of a pair of pulses of light. *Phys. Rev. A* **69**, 043801, DOI: [10.1103/PhysRevA.69.043801](https://doi.org/10.1103/PhysRevA.69.043801) (2004).
9. Vewinger, F., Appel, J., Figueroa, E. & Lvovsky, A. I. Adiabatic frequency conversion of optical information in atomic vapor. *Opt. Lett.* **32**, 2771–2773, DOI: [10.1364/OL.32.002771](https://doi.org/10.1364/OL.32.002771) (2007).
10. Park, K.-K., Zhao, T.-M., Lee, J.-C., Chough, Y.-T. & Kim, Y.-H. Coherent and dynamic beam splitting based on light storage in cold atoms. *Sci. Reports* **6**, DOI: [10.1038/srep34279](https://doi.org/10.1038/srep34279) (2016).
11. Li, Z., Xu, L. & Wang, K. The dark-state polaritons of a double- Λ atomic ensemble. *Phys. Lett. A* **346**, 269 – 274, DOI: <https://doi.org/10.1016/j.physleta.2005.08.009> (2005).
12. Viscor, D. *et al.* Two-color quantum memory in double- Λ media. *Phys. Rev. A* **86**, 053827, DOI: [10.1103/PhysRevA.86.053827](https://doi.org/10.1103/PhysRevA.86.053827) (2012).
13. Tsai, P.-J., Wei, Y.-C., Wu, B.-H., Lin, S.-X. & Chen, Y.-C. Theoretical study of a memory-based optical converter with degenerate zeeman states. *Phys. Rev. A* **100**, 063843, DOI: [10.1103/PhysRevA.100.063843](https://doi.org/10.1103/PhysRevA.100.063843) (2019).
14. Guan, P.-C., Chen, Y.-F. & Yu, I. A. Role of degenerate zeeman states in the storage and retrieval of light pulses. *Phys. Rev. A* **75**, 013812, DOI: [10.1103/PhysRevA.75.013812](https://doi.org/10.1103/PhysRevA.75.013812) (2007).
15. Hsiao, Y.-F. *et al.* Highly efficient coherent optical memory based on electromagnetically induced transparency. *Phys. Rev. Lett.* **120**, 183602, DOI: [10.1103/PhysRevLett.120.183602](https://doi.org/10.1103/PhysRevLett.120.183602) (2018).
16. Hsiao, Y.-F., Chen, H.-S., Tsai, P.-J. & Chen, Y.-C. Cold atomic media with ultrahigh optical depths. *Phys. Rev. A* **90**, 055401, DOI: [10.1103/PhysRevA.90.055401](https://doi.org/10.1103/PhysRevA.90.055401) (2014).
17. Gorshkov, A. V., André, A., Fleischhauer, M., Sørensen, A. S. & Lukin, M. D. Universal approach to optimal photon storage in atomic media. *Phys. Rev. Lett.* **98**, 123601, DOI: [10.1103/PhysRevLett.98.123601](https://doi.org/10.1103/PhysRevLett.98.123601) (2007).
18. Harris, S. E. & Yamamoto, Y. Photon switching by quantum interference. *Phys. Rev. Lett.* **81**, 3611–3614, DOI: [10.1103/PhysRevLett.81.3611](https://doi.org/10.1103/PhysRevLett.81.3611) (1998).
19. Steck, D. A. Cesium d line data, <https://steck.us/alkalidata/cesiumnumbers.1.6.pdf> (1998).

Acknowledgements

This work was supported by the Ministry of science and technology of Taiwan under grant numbers MOST 108-2112-M-001-030-MY3 and MOST 108-2639-M-007-001-ASP. We also thank the supports from National Center for Theoretical Sciences of Taiwan under ECPI program and Center for Quantum Technology of Taiwan.

Author contributions statement

YC W. and SX L. conducted the experiment and analysed the data. YC W. and PJ T. established the theory. YC W. and YC C. wrote the manuscript. All authors reviewed the manuscript.

Additional information

Accession codes (where applicable); **Competing interests** The authors declare no competing interests.